Coherent Quantum Network of Superconducting Qubits as a Highly Sensitive Detector of Microwave Photons for Searching of Galactic Axions

Fig. 1. Schematic of a setup in which an SQN composed of N flux qubits coupled to a low-dissipative resonator (on the bottom) and a transmission line (on the top) (from).

large number of qubits (N) and utilization of a collective mode established in SQNs with a long-range coupling between qubits, it is possible to exceed the standard quantum limit and reach the so-called Heisenberg limit of sensitivity and the SNR is proportional to N instead of $\sim\sqrt{N}$ in case of N non-interacting qubits . Practical realization of the detector requires the embedding of an SQN into a low-dissipative resonator in which microwave photons arrive, and a transmission line for measuring of the frequency dependent transmission coefficient demonstrating resonant drops at the qubit's frequencies. We formulated the quantum-mechanical theoretical model in the general case of disordered interacting SQNs. We obtained that an amplitude of the main resonance drastically increases as the interaction between qubits overcomes the disorder and the collective state is formed. In addition, in the presence of a weak non-resonant photon field, the positions of resonant drops depend on the number of photons, i.e., the collective AC Stark effect is theoretically predicted . T-type SQNs detectors with 10 flux qubits were designed, fabricated, and tested at ultra-low temperatures in terms of microwave measurements of scattering parameters and two-tone spectra. A substantial shift of the frequency position of the resonant drop of the transmission coefficient induced by the pump tone signal was observed by two tone measurements. This frequency shift clearly manifests a nonlinear multiphoton interaction between a second-tone microwave pump signal and an array of qubits.

As for the calibration method of the SQN detector by single photons in microwave range, we plan to use the heralding approach based on the generation of correlated photons pairs, where the detection of one photon of the pair "heralds" the existence of the other photon. In this context, the application of Josephson Travelling Wave Parametric Amplifiers (JTWPAs) for development of the heralded single-photon source is discussed.

II. Theory

A. General Theoretical Description of SQN As a Single Photon Detector

We consider a set of N identical waveguides each containing M identical qubits, into which an input signal consisting of either 0 or 1 photons is uniformly fed (see Fig. , Ref.). The photons interact with the qubits while travelling through the waveguides, the interaction term proportional to $\sigma_z a^+ a$. A single photon will induce the rotation of the qubit state about the axis O_z by an angle $\theta = h_p \tau$, where τ is the effective passage time, and h_p characterizes the interaction of qubits with the photon field in the dispersive regime. Even in the absence of direct qubit-qubit interactions, qubits will be interacting through the vacuum waveguide mode, producing the rotation of the qubit quantum state about the axis O_x by an angle $\Delta = h_\delta \tau << 1$. Noise is included in the model by replacing the photon operator a with $a' = \sqrt{\eta}a + \sqrt{(1\text{-}\eta)}b$, where b is the noise field operator and $\eta < 1$ is the quantum efficiency. Direct qubit-qubit interactions are taken into account through the terms proportional to $\sigma_{zi}\,\sigma_{zj}$..

For the uncorrelated initial qubit state, and in the absence of direct qubit-qubit interaction, and with $\Delta << 1$, the SNR scales as $\sqrt{M}$ (that is, proportional to the number of qubits in a single waveguide), and no better than $\sqrt{N}$ (the number of waveguides). Therefore, the optimal SNR scaling is achieved in the case of a single waveguide ($N = 1$, $n = M$) and corresponds to the standard quantum limit.

This result is improved by switching direct qubit-qubit interactions. Remarkably, nearest-neighbour interactions are not effective . Otherwise, the Heisenberg limit is achieved in case of infinitely strong coupling ("giant spin" limit) between all qubits, with SNR scaling as n. This condition is met when the average zz-coupling between the qubits greatly exceeds their coupling to the field. Intermediate coupling strengths produce gradual transition between n and $\sqrt{n}$ dependences.

B. Theory of an SQN Interacting With a Microwave Photon Field: AC Stark Effects

Here, we present a theoretical study of *coherent collective quantum states* obtained in *disordered* superconducting qubits networks (SQNs) interacting with a photon field of low-dissipative resonator (see Fig.).

1) Collective Quantum States in Coherent Network of Interacting Superconducting Qubits: Collective AC Stark Effect (Low Photon Numbers): An SQN is composed of a large number of superconducting qubits characterized by qubits frequencies, ω_i. The frequencies of individual qubits can differ significantly from each other due to the presence of an unavoidable spread of qubits physical parameters. Coupling of an SQN to a low-dissipative resonator (see, Fig.) provides an effective long-range exchange interaction between all qubits. The origin of such interaction is an exchange (absorption and emission) of virtual photons between well separated qubits.

Deriving a total Hamiltonian H_{SQN} for a setup presented in Fig. , and using the exact numerical diagonalization of H_{SQN} the Fourier transform of temporal correlation function of the total polarization, $C(\omega)$, was obtained . Coupling of an SQN to the transmission line allows one to experimentally access $C(\omega)$ by measuring of the corresponding transmission coefficient $S_{21}(\omega)$. As the interaction strength becomes larger than a spread of individual qubits frequencies, the collective excited state forms, and a single large resonance with the amplitude proportional to N-number of qubits is obtained in $C(\omega)$.

Next, we theoretically study the coherent quantum dynamics of SQNs in the presence of a weak (a few photons) *non-resonant* microwave radiation providing different photon states ($|0\rangle$, $|1\rangle$, and $|2\rangle$) in a low-dissipative resonator. In this regime, we

obtain a few dominant resonances in *C(ω),* whose frequency *positions* depend on the number of photons, i.e., the *collective ac Stark effect* is obtained . Such frequency shift can be used for resolving photon number states with a high accuracy and employing SQNs as sensitive single-photon detectors.

2) Qubits Controlling Coupling Between Two Low-Dissipative Resonators: Multiphoton AC Stark Shift of the Resonator Frequency: Consider N qubits, where ith qubit has excitation frequencies ω_i, each being in contact with the R-resonator with frequency ω_R. Denoting the detuning $\Delta_i = -\omega_i + \omega_R$, the R-resonator-qubit coupling g_i, and the Rabi frequency ϵ, we find the frequency of the T-resonator as $\omega(\epsilon) = \omega_R + \sum_{i=1}^{N} g_i^2 \Delta_i^2/(\Delta_i^2 + \epsilon^2)^{3/2}$. Note that the frequency shift between zero and high pumping power, $\Delta\omega = \sum_{i=1}^{N} g_i^2/|\Delta_i|$, provides information about the qubits, which are primarily involved in the photon tunneling processes. This frequency shift is the sum of the multiphoton AC Stark shift values of each qubit.

3) Nonlinear Response of an SQN Embedded in two Low-Dissipative Resonators: The Quantum Superposition of Two Nonequilibrium Photonic States: As the detuning $\Delta_i >> \omega_i$ the SQN coupled to the low-dissipative resonator can demonstrate strong nonlinear effects due to multiphoton excitation of upper energy levels of qubits , , . Including such multiphoton excitations of qubits we derive the equation for number of photons *n* collected in the R-resonator in the presence of external resonant microwave radiation of power *P* and frequency ω_d: $n[(\omega_d - \omega_R + g_R\ n)^2 + \gamma^2] = kP$, where g_R is the coupling coefficient between SQN and R-resonator; γ is a low dissipation of a system. Thus, such a system can support *two* nonequilibrium states with low, $n \sim P$, and high, $n = (\omega_R - \omega_d)/g$, number of photons. These nonequilibrium states , and their quantum superposition , that can be expected at extremely low temperatures and dissipation, have to manifest themselves in the resonance frequency shift of the T-resonator coupled to an SQN: $\omega_T = \omega_R - g_T\ n$, where g_T is the coupling coefficient between SQN and T-resonator.

III. Experiment

A. Sample Fabrication

The T-type architecture was developed to achieve the conditions required by the theoretical proposal of Zagoskin et al. , namely two spatially separated resonators of the same resonant frequency coupled to an array of superconducting qubits. In practice, the array of flux qubits is coupled to the electric field of the one and to the magnetic field of the other resonator. We limited the size of the qubit structures to avoid an increase in geometric coupling, such that for realizing an increased number of ten qubits the shunting capacitances have been reduced. The optical image of the SQN device with 10 flux qubits is shown in Fig. . Sequences of zoomed SEM pictures of fabricated sample are shown in Fig. – . The first resonator, T-resonator between port 1 and port 2 in Fig. is delimited by two capacitors of about 5 fF each. The second resonator, R-resonator with input port 3 in Fig. is terminated with one capacitor of about 5 fF on one side and is capacitively coupled to the flux qubits on the other side (Fig.). The capacitors of three ports are also reported in Fig. . The T configuration guarantees inductive and capacitive couplings to the flux qubits of the T and R resonators, respectively, and an electrodynamic isolation between them in absence of flux qubits. With proper design, the coupling between T and R resonators is provided by the qubit system embedded inside the coplanar capacitor (Fig.). The calculated frequencies of the T-resonator modes (port 1-port 2 connection) are shown in Table .

The T and R resonators are fabricated by depositing a 200 nm thick Nb film on a silicon substrate that is structured by the RIE. The flux qubits are made of Al Josephson-junctions fabricated by two angle shadow evaporation technique. Every flux qubit of the SQN consists of a 6x4.5 μm^2 loop with three Josephson junctions. Two junctions are designed to have identical size of 0.2x0.87 μm^2 while the third is scaled by a factor $\alpha < 1$ (see

Fig. 2. (a) Optical image of the T-type SQN with 10 C-shunted flux qubits with two resonators. Port's numbers are indicated. (b)-(d) SEM images of magnified parts indicated by green: (b) It is clearly possible to see the coplanar capacitor which connects the R-resonator with the T-resonator. The 10 C-shunted flux qubits are embedded inside the coplanar capacitor. (c) Five flux qubits shunted by coplanar capacitors. (d) Zoomed SEM image of the flux qubit loop.

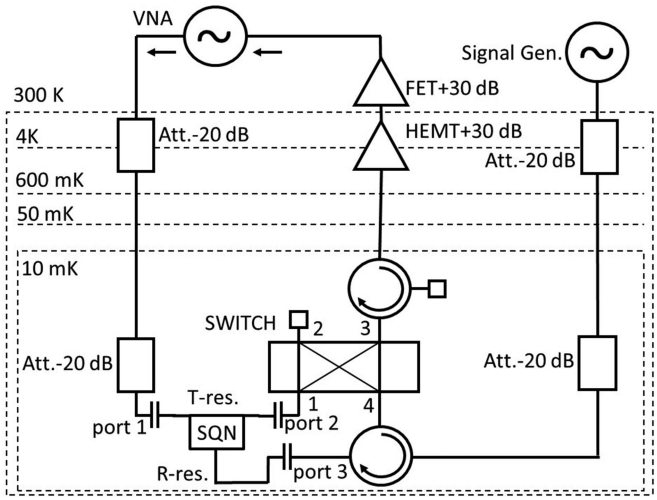

Fig. 3. Microwave experimental setup.

TABLE I
LIST OF CALCULATED T RESONATOR MODES AND QUALITY FACTORS

Mode	Frequency (GHz)	Loaded quality factor
$\lambda/2$	2.6188	56722
λ	5.2376	33851
$3/2\lambda$	7.8564	23407

Fig.). For qubits of the SQN measured here, the factor $\alpha = 0.8$. Samples have been fabricated with an critical current density of 80 A/cm^2 ensuring the simulated energy level splittings as required by the planned measurement protocols. Details on the qubit fabrication process, frequencies and decoherence rate of individual flux qubits can be found in . Each flux qubit is shunted by coplanar capacitors (Fig.).

B. Experimental Setup

Measurements of fabricated T-type SQN were carried out at the Laboratori Nazionali di Frascati (LNF) (Italy) in a Leiden Cryogenics CF-CS110-1000 dilution refrigerator at temperature of 15 mK. The microwave experimental setup is shown in Fig. . We used two instruments providing rf signals, a signal generator Rohde&Schwarz SMA100B serving to apply a second tone pump signal to port 3 and the Vector Network Analyzer (VNA) Agilent E5071C to measure scattering parameters both T-Resonator and R-Resonator. Their outputs (first port of the VNA) are directed to two different rf lines going down into the cryostat. The input rf line is interrupted with a 20 dB power attenuator at 4 K and with another 20 dB attenuator at 10 mK, to reduce the thermal power coming from the hottest plates and environments. The total attenuation, including the losses in the coaxial cables, is about 60 dB between 5 and 10 GHz. Before reaching the device, the input line encounters a cryogenic circulator (bandwidth 4–12 GHz). This allows directing the signal coming from the R-resonator, either transmitted or reflected, to the amplification stage in the output line. A cryogenic switch is used to direct the output signal from the R or T resonator to the amplification stage. The other signal is terminated to a 50 Ω load. A second circulator avoids reflected power from the HEMT amplifier back into the device. The HEMT amplifier, located at the 4 K stage, and the FET amplifier at room temperature give a total amplification of 60 dB. Then, a splitter equally divides the output power: one half is sent to the second port of the VNA for S_{21} measurements and one half to the Signal Hound SM200B spectrum analyzer for power-spectrum measurements.

The SQN device was bonded on the sample holder. The sample holder has six SMA connectors for input and output of rf signals and several dc lines reachable through the USB-c connectors for device bias and dc characterizations. A superconducting coil, made of a single filament of NbTi superconductor clad with copper of 0.4 mm diameter, was wound around the sample holder lid.

Fig. 4. (a)- First-tone through-transmission S_{21} vs VNA-frequency dependencies recorded at different powers of the second-tone signal of frequency of 7.743 GHz applied to the port 3. Experiment was done in zero magnetic field at T = 15 mK. (b)- Dependence of the frequency position of the resonant drop reported in (a) as a function of the power of the second-tone signal.

C. Scattering Parameter Measurements

We characterized the three-port T-type SQN in zero magnetic field by measuring the scattering parameters with the VNA. We looked for the resonances of the first three modes listed in Table . By changing both input port and the output lines by the cryogenic switch, we were able to measure both the through (port 1- port 2 connections) and cross (port 1 -port 3 connections) transmission coefficients S_{21}, as well as the reflection on port 3 (port numbers are reported in Fig.).

The through transmission S_{21} of the T-resonator shows a clear Lorenz peak at frequency 2.687 GHz with quality factor of 55500 which is close to the theoretical value reported in Table . We found large resonant drops in the reflection coefficient on port 3 S_{33}, at slightly lower frequencies of those of Table . (at 2.581 GHz, 5.162 GHz and 7.743 GHz in the experiment). This substantial shift of resonant frequencies can be explained by the coupling between qubits of the SQN and resonators.

D. Two -tone Spectral Measurement of the T-type Three Port SQN Device

In these experiments the frequency of the VNA was chosen close to the third -harmonic resonant drop of the R-resonator (7.74 GHz). We set the VNA output-power to -40 dBm, corresponding to about -100 dBm at the device and measured the through transmission (S_{21}) between port 1 and port 2. At the same time, we sent a second tone of frequency 7.743 GHz to the R-resonator to the port 3, and varied the output power of the generator from -50 dBm to -20 dBm which corresponds to effective power applied to the port 3 from -110 dBm to -80 dBm. By increasing the second tone power we clearly observe a variation of the resonant drop frequency in the through transmission-spectrum S_{21} (see Fig.). The dependence of the frequency positions of the resonant drop on the power of a second tone signal is shown in Fig. . As one can see from Fig. the frequency position of the resonant drop decreases substantially with the pump power. We note that the frequency position of the resonant drop of the through transmission S_{21} varies with the frequency of the second-tone pump signal applied to port 3 at constant power of -25 dBm.

Experimental results presented in Fig. show a substantial shift of the resonant frequency of T-resonator with power P of

an external microwave radiation applied to the R-resonator. Such a shift can be qualitatively explained in the framework of two different models: multiphoton AC Stark effect of an SQN (see Section) or multiphoton excitations of upper levels of an SQN (see Secion). Detailed quantitative comparison of experiments and elaborated models will be presented elsewhere.

IV. Detector Calibration Via Heralding

Calibration of the SQN detector by microwave single photons is a non-trivial task. For this aim we apply the approach inherited from nonlinear optics, which consists in generation of correlated photons pairs, where the detection of one photon of the pair "heralds" the existence of the other photon . We develop the JTWPAs consisting of many cells in series containing non-linear elements with a Josephson-based core as a heralded single-photon source . The correlated photon pairs produced in JTWPA open the way to a fundamentally absolute method to calibrate a microwave single-photon detector: using coincidence-measurement techniques, the heralded single photon sources can be applied to the calibration of the detector without the need for an absolute radiometric reference .

V. Conclusion

We presented a new proposal to detect low power microwave signal (a few GHz) based on a coherent collective response of quantum states occurring in superconducting interacting qubits networks (SQNs). A theoretical description of a single microwave photon detector based on moderated size network of interacting superconducting qubits was developed. Design of the layout of T-type three port SQN detectors containing 10 flux qubits was provided and the samples were fabricated by Al-based technology with Nb resonator. Scattering parameters measurements and two tone spectra experiment were carried out at zero magnetic field and ultra-low temperatures. A substantial shift of the resonant drop in the transmission coefficient induced by the pump second-tone signal was observed, and this effect presents experimental evidence of a nonlinear multiphoton interaction between the pump signal and flux qubits of the SQN. Application of the JTWPA as a heralded single-photon source for the calibration of the SQN detector via heralding is finally considered.

References

[1] N. Du et al., "Search for invisible axion dark matter with the axion dark matter experiment," *Phys. Rev. Lett.*, vol. 120, no. 15, 2018, Art. no. 151301.

[2] A. L. Pankratov, L. S. Revin, A. V. Gordeeva, A. A. Yablokov, L. S. Kuzmin, and E. Il'ichev, "Towards a microwave single-photon counter for searching axions," *npj Quantum Inf.*, vol. 8, pp. 61/1–61/7, May 2022, doi: .

[3] D. I. Schuster et al., "Resolving photon number states in a superconducting circuit," *Nature*, vol. 445, pp. 515–518, Feb. 2007 doi: .

[4] A. M. Zagoskin et al., "Spatially resolved single photon detection with a quantum sensor array," *Sci. Rep.*, vol. 3, 2013, Art. no. 3464, doi: .

[5] S. Zhou, M. Zhang, J. Preskill, and L. Jiang, "Achieving the Heisenberg limit in quantum metrology using quantum error correction," *Nature Commun.*, vol. 9, 2018, Art. no. 78.

[6] M. V. Fistul, O. Neyenhuys, A. B. Bocaz, M. Lisitskiy, and I. M. Eremin, "Quantum dynamics of disordered arrays of interacting superconducting qubits: Signatures of quantum collective states," *Phys. Rev. B*, vol. 105, 2022, Art. No. 104516.

[7] P. Navez, A. G. Balanov, S. E. Savel'ev, and A. M. Zagoskin, "Toward the Heisenberg limit in microwave photon detection by a qubit array," *Phys. Rev. B*, vol. 103, 2021, Art. no. 064503.

[8] M. I. Dykman and M. V. Fistul, "Multiphoton antiresonance," *Phys. Rev. B*, vol. 71, 2005, Art. No. 140508(R).

[9] P. Jung et al., "Multistability and switching in a superconducting metamaterial," *Nature Commun.*, vol. 5, no. 1, 2014, Art. no. 3730.

[10] N. Maleeva et al., "Circuit quantum electrodynamics of granular aluminum resonators," *Nature Commun.*, vol. 9, 2018, Art. no. 3889.

[11] G. Oelsner, U. Hubner, S. Anders, and E. Il'ichev, "Application and fabrication aspects of sub-micrometer-sized Josephson junctions," *Low Temp. Phys.*, vol. 43, no. 7, pp. 779–784, Jul. 2017.

[12] G. Brida et al., "An extremely low-noise heralded single-photon source: A breakthrough for quantum technologies," *Appl. Phys. Lett.*, vol. 101, 2012, Art. no. 221112, doi: .

[13] M. R. Perelshtein et al., "Broadband continuous variable entanglement generation using Kerr-free Josephson metamaterial," *Phys. Rev. Appl.*, vol. 18, 2022, Art. no. 024063, doi: .

[14] G. Brida, S. Castelletto, I. P. Degiovanni, and C. Novero, and M. L. Rastello, "Quantum efficiency and dead time of single-photon counting photodiodes: A comparison between two measurement techniques," *Metrologia*, vol. 37, pp. 625–628, 2000.

Open Access funding provided by 'Consiglio Nazionale delle Ricerche-CARI-CARE-ITALY' within the CRUI CARE Agreement